Exploiting Different Electricity Markets via Highly Rate-Mismatched Modular Electrochemical Synthesis

Rui Wang[1], Jiaze Ma[2], Hongyuan Sheng[1], Victor M. Zavala[2*], Song Jin[1*]

[1] Department of Chemistry, University of Wisconsin-Madison, 1101 University Avenue, Madison, Wisconsin 53706, USA.

[2] Department of Chemical and Biological Engineering, University of Wisconsin-Madison, 1415 Engineering Dr, Madison, WI 53706, USA.

*Corresponding author. Email: victor.zavala@wisc.edu; jin@chem.wisc.edu

Abstract: Mitigating the inherent spatio-temporal stochasticity and intermittency of renewable power is key for enabling the decarbonization of the power grid and motivates the development of flexible technologies that can shift power demand/supply across space-time and scales. Here, we develop a new electrochemical synthesis strategy capable of providing demand flexibility at different timescales by participating in multiple electricity markets (day-ahead, real-time, and frequency regulation). Using a fast proton redox material, copper hexacyanoferrate, highly rate-mismatched modular electrochemical synthesis was achieved by decoupling half-reactions with different intrinsic kinetics to produce chemicals under drastically different reaction rates and timescales: the fast hydrogen evolution reaction and slow persulfate production reaction. Such a strategy enables flexible participation in different electricity markets and can reduce electricity cost by 30-40%. These results open a new conceptual strategy for flexibly integrating modular electrochemical processes into the fluctuating power grid to achieve more economical and sustainable operations.

.

One-Sentence Summary: Modular electrochemical synthesis flexibly participates in dynamic electricity markets and reduces cost dramatically.

Main Text:

Decarbonizing the power grid requires the widespread adoption of renewable (wind/solar) power sources(*1, 2*). Mitigating the unpredictable and intermittent nature of renewable power presents a grand challenge, driving the unprecedented restructuring of the power grid. The multi-scale and spatio-temporal behaviors from this restructuring will require the power grid to harness flexibility in diverse forms and enable a reliable and sustainable power supply to society(*3, 4*). Lack of power grid flexibility is currently manifesting as large amounts of renewable power that remain stranded (cannot be absorbed by the grid) or even the curtailment of renewable electricity generation(*5, 6*); stranded power is projected to grow as more renewable power is injected into the grid and hinders the ability to decarbonize the grid(*4*). Independent system operators (ISOs) operate different electricity markets to harness and remunerate flexibility provided at different times and network locations(*7*). For instance, in markets such as the day-ahead market (DAM) and real-time market (RTM), electricity prices are updated every hour or 5-15 minutes to promote balancing of power supply and demand (Fig. 1A). The frequency regulation (FR) market is a critical ancillary service market that operates at a 2 second time resolution, and is designed to secure balancing at fast timescales(*7*). The need for FR services continues to increase as more renewable power is absorbed in the grid. The price signals from these markets, particularly negative prices resulting from stranded power, indicate when and where resources are most valuable and provide an economic incentive for technologies that can use/supply power(*8*). Therefore, flexible technologies that can participate in markets at different times/locations can help the grid absorb more wind/solar power and economically monetize this service(*9*).

Various technologies have been developed to handle power fluctuations in the grid, such as hydroelectric storage (PHES)(*10, 11*), compressed air energy storage (CAES)(*12, 13*), battery systems(*14, 15*), and power to gas (P2G)(*16, 17*) (Fig. 1B). These technologies could strategically convert excess power from the grid (or power at low or negative prices) into potential or chemical energies, and then use stored energies during power scarcity (or power at high prices). Compared to PHES or CAES with long storage/operation timescale, electrochemical technologies with a short storage/operation timescale, especially P2G, can lead to spatially distributed power demands and new sources of flexibility. Recent results show that incorporating proton exchange membrane electrolysis capable of flexible participation in DAM and RTM to produce hydrogen in methanol synthesis processes can lower the hydrogen cost by 31% from that via the conventional steam-methane reforming process(*18*). However, a fundamental issue of such an electrochemical system with coupled half-reactions is that the slow reaction constrains the system response; from a power grid perspective, this can limit the system's ability to respond to signals that are faster than the limiting time constant. The mismatch between the timescales of paired half-reactions can also lead to system inefficiencies (parasitic reactions)(*19, 20*). Instead of the coupled electrochemical system, decoupling paired reactions using redox-active materials(*21-26*) or redox reservoirs (RRs)(*27-29*) allows for flexible pairing of different half-reactions potentially to participate in different electricity markets. In principle, using such a strategy, half-reactions can be performed at desired rates and under various timescales to provide more design flexibility for participation in different electricity markets and process modularization of chemical supply chains.

Here, we present a highly rate-mismatched modular electrochemical synthesis (ModES) process that can effectively participate in DAM, RTM, and FR markets (Fig. 1C) and reduce electricity costs. We decouple the conventionally tightly coupled hydrogen evolution reaction (HER) with fast kinetics and persulfate production reaction (PSR) with slow kinetics and use a redox reservoir (RR) electrode with fast kinetics to separately pair with these two half reactions.

The electricity in spikes of a few seconds at a low or even negative price can be used to produce H_2 and charge the RR electrode quickly. The electrons/ions stored in the RR electrode enable slower persulfate ($S_2O_8^{2-}$) production over a few minutes. A proton battery material that shows fast proton transport and storage via the Grotthuss mechanism, copper hexacyanoferrate (CuHCF), is demonstrated as the RR electrode with excellent rate capability and cycling stability even in mismatched charging/discharging conditions. The developed computational modeling framework shows that this highly rate-mismatched ModES system operating under a flexible power load could reduce electricity costs by 30-40% compared to the baseline and even generate revenues by participating in the FR market. These results confirm the promise of modular electrosynthesis for dynamic electricity markets and show how flexible electrochemical systems can open new revenue opportunities.

Design of the highly rate-mismatched ModES system

We design a highly rate-mismatched ModES system to produce value-added chemicals under different timescales to participate in dynamic electricity markets. The key to such a system is the use of solid-state redox materials that can achieve fast storage/release of electrons and ions and decouple electrochemical half-reactions with different intrinsic kinetics. As the initial demonstration, we choose HER, one of the fastest electrochemical reactions that produces green hydrogen fuel, as the model reaction to participate in the FR market, and PSR, a widely used electrosynthesis with slow intrinsic kinetics (estimated market size of $750 million in 2027)(*30*), as the other model reaction to participate in DAM and RTM. Compared to conventional persulfate production (fig. S1), here flexible HER and PSR with different reaction rates are achieved in a membrane-free, decoupled fashion mediated by a RR electrode (Fig. 1C): proton-consuming HER pairs with the oxidation of RR that releases protons at a fast reaction rate. Then the reduction of RR that uptakes protons pairs with the slower PSR in the other electrochemical cell. The RR electrode can transport protons from the PSR cell ($Cell_{S_2O_8^{2-}}$) to the HER cell ($Cell_{H_2}$) to maintain proton balance. Because dynamic electricity markets exhibit price fluctuations at different timescales across seconds to hours, stable RRs with fast kinetics and selective proton transport must be developed for highly rate-mismatched electrochemical productions.

Synthesis and electrochemical performance of the fast proton battery material

The rate capability of energy storage materials is strongly influenced by the charge carriers. Compared to metal ions, protons have a smaller mass and ionic radius and exhibit fast diffusion kinetics via the unique Grotthuss mechanism (Fig. 2A)(*31, 32*), where proton jumps from one water molecule to the next through the hydrogen-bonding network(*33*). Moreover, redox materials with defects(*34, 35*) or large tunnels(*36*) may form inner hydrogen-bonding networks and achieve fast Grotthuss conduction inside solids. Therefore, we choose Prussian Blue analog copper hexacyanoferrate (CuHCF) with an open-framework structure that could be filled with a crystal water network(*37*), which showed promise for fast redox kinetics(*38*).

Nanostructured CuHCF material (Fig. 2B) was synthesized via a co-precipitation method (see Methods for details). The characteristic (200), (220), and (400) powder X-ray diffraction (PXRD) peaks of the CuHCF material match well with the standard pattern of the cubic PBA phase (JCPDS No. 52-1907) (fig. S2). Thermogravimetry analysis (TGA, fig. S3) and inductively coupled plasma optical emission spectroscopy (ICP-OES, table S1) reveal the water content and element compositions of the as-synthesized CuHCF material, which yield the chemical formula of $K_{0.06}Cu_{1.5}[Fe(CN)_6] \cdot 5.5\ H_2O$.

We then studied the electrochemical behaviors of the CuHCF material in 2 M H_2SO_4 solution. Cyclic voltammograms (CVs) showed four pairs of reversible redox peaks, where O1/R1 was attributed to Cu^{II}/Cu^{I} and other peaks were from Fe^{III}/Fe^{II} (Fig. 2C)(*39, 40*). The peak current in CVs, *I*, was analyzed based on equation $I = av^b$, where *a* was the coefficient and *v* was the scan rate. The *b* values for the anodic peaks (Fig. 2D) and cathodic peaks (fig. S4) were close to unity, indicating strong capacitive behaviors with fast kinetics(*41, 42*). The CuHCF electrodes exhibited excellent capacity retention of 75.3 % at even 1500 C rate (a short (dis)charge period < 2 s) (Fig. 2E and table. S2). Note that the *n*C rate means that the (dis)charge period of the electrode is 1/*n* hours, and the 1 C rate is defined as 65 mA g^{-1} based on the theoretical capacity of CuHCF (65 mAh g^{-1}). The linearly increasing potential hysteresis of CuHCF with increasing current densities (fig. S5) revealed that its rate capability was limited by uncompensated resistance in the electrochemical cell rather than the kinetics of proton storage/release. Galvanostatic cycling tests confirmed the long-term stability of CuHCF at 1 A g^{-1} (15 C) with 0.006 % decay per cycle (fig. S6A) and at 5 A g^{-1} (75 C) with 0.005 % decay per cycle (fig. S6B).

We further evaluated the capacity and Coulombic efficiency (CE) of CuHCF at mismatched charging/discharging rates. No matter how fast the charging rate was, CuHCF showed CE above 90 % when the discharging rate was above 1.5 C (Fig. 2F and fig. S7). Reduced CE might result from the self-discharge of the electrode at a high charging rate (fig. S8). The CuHCF electrode also showed capacity retention above 78% (compared to the capacity at 1 C rate) and good cycling stability at mismatched rates if the ratio of the charging rate/discharging rate stayed below 500 (Fig. 2G and fig. S9). These results suggest that rate-mismatched production of persulfate and hydrogen with a time ratio from 1:1 to 100:1 should be achievable with a high CE and capacity retention using the CuHCF electrode (Fig. 2H). Specifically, when the time ratio of PSR to HER is 100:1 with an HER rate of 1000 C and a PSR rate of 10 C, the HER reaction would finish in 2 s to enable its participation in FR market to receive flexibility incentives. The excellent long-term stability and fast proton transport suggest the suitability of CuHCF for rate-mismatched electrochemical productions.

Investigation of HER and PSR in conventional electrolysis

We first separately investigated HER and PSR in 2 M H_2SO_4 solution considering their fast kinetics and high efficiency in acidic solutions(*43*). Pt electrode, widely studied for acidic HER(*44*), was chosen as the catalytic electrode for H_2 production. The linear sweep voltammetry (LSV) curve of the Pt electrode shows an overpotential as low as 43 mV to achieve the current density of 10 mA cm^{-2} (fig. S10A). Chronoamperometry curves at different applied potentials show nearly constant currents without noticeable decay (fig. S10B), suggesting excellent catalytic stability.

To minimize the competitive oxygen evolution reaction (OER) and possible chemical corrosion(*43, 45, 46*), we chose a stable boron-doped diamond (BDD) electrode with a high overpotential for OER and a good activity for PSR (see details on electrode fabrication in Materials and Methods and fig. S11). The LSV curve of the BDD electrode shows an increased anodic current density with increasing applied potential and a high current density of 85 mA cm^{-2} at 3.10 V vs. standard hydrogen electrode (SHE) (fig. S10C). As the applied potential increases, the Faradaic efficiency of PSR [FE ($S_2O_8^{2-}$)] increases and reaches above 80 % when the applied potential is above 2.84 V vs. SHE (figs, S10C, D, and 12). Moreover, stable bulk PSR electrolysis over the BDD electrode can accumulate $S_2O_8^{2-}$ (fig. S10D), confirming the excellent activity and stability of the BDD electrode.

Highly rate-mismatched ModES production of hydrogen and persulfate

We then demonstrated a prototype rate-mismatched ModES production of H_2 and $S_2O_8^{2-}$ mediated using a CuHCF RR electrode in two electrochemical cells (Fig. 3A, see Materials and Methods for details). During rate-mismatched ModES cycles (Fig. 3B and fig. S13), in $Cell_{H_2}$, HER at the Pt electrode accompanies the oxidation of RR that releases protons; then in $Cell_{S_2O_8^{2-}}$, PSR at the BDD electrode accompanies the reduction of RR that uptakes protons. Here, we assume the FE of HER to be 100 % since the only possible product during the cathodic reaction is H_2. The FE ($S_2O_8^{2-}$) was calculated based on the measured concentration of the produced persulfate in $Cell_{S_2O_8^{2-}}$. During ModES cycles, the average potential difference between the catalytic and RR electrodes determines the average cell voltages (V_{cell}). To describe the energy utilization of the ModES, we use the voltage efficiency (VE) defined for decoupled aqueous electrosynthesis(*27, 29*) based on the following equation:

$$VE(\%)= V_{DIR}/ V_{ModES} \times 100\% = (V_{S_2O_8^{2-}}+ V_{H_2}-\Delta V) / (V_{S_2O_8^{2-}}+ V_{H_2}) \times 100\%$$

where V_{DIR} is the potential difference between the HER at the Pt electrode and PSR at the BDD electrode, respectively; ΔV represents the difference between the average potential of the RR electrode in $Cell_{H_2}$ and $Cell_{S_2O_8^{2-}}$.

We started ModES production of H_2 and $S_2O_8^{2-}$ from equal rates of HER /PSR and finally achieved a high mismatched production rate (100:1) of HER /PSR: the PSR rate was kept at 10 C based on the capacity of the CuHCF RR electrode, and the HER rate increased from 10 C to 1000 C. During the first 5 cycles with equal rates, the average RR potentials (E_{RR}) in both cells were nearly 1.0 V vs. SHE (Fig. 3C), and the ΔV was only 20 mV (fig. S14), confirming the fast proton kinetics of CuHCF. The corresponding V_{cell} showed repeatable values of 1.00 V and 1.91 V with fluctuations less than 10 mV in $Cell_{H_2}$ and $Cell_{S_2O_8^{2-}}$. Moreover, an average CE of RR of 99.4 %, VE of 99.7 %, and FE ($S_2O_8^{2-}$) of ~75 % (Fig. 3D) indicate the high energy efficiency of the ModES system. During cycles 6 to 10 when the HER rate increased to 100 C, E_{RR} and V_{cell} in $Cell_{H_2}$ increased by about 20 mV and 90 mV (Fig. 4C and fig. S15), respectively, which could be attributed to the iR drop of the RR electrode and overpotential for HER. The E_{RR} and V_{cell} in $Cell_{S_2O_8^{2-}}$ showed nearly no change. The average CE of RR, VE of the system, and FE ($S_2O_8^{2-}$) were like those seen in cycles 1-5, confirming that RR enabled a stable decoupled operation at a 10:1 ratio of the HER rate/PSR rate.

We then performed highly rate-mismatched ModES production at the HER rates of 500 C and 1000 C and the PSR rate of 10 C, using a smaller CuHCF RR electrode. When the ratios of mismatched rates were 50:1 and 100:1, fast HER can be achieved in 4.77 s (Fig. 3B and fig. S16) and 1.87 s (Fig. 3B and fig. S17), respectively, in agreement with the rate-mismatched cycling results of the CuHCF electrode (Figs. 2Fand G). The E_{RR} decreased by about 70 mV in $Cell_{S_2O_8^{2-}}$ and increased only about 170 mV in $Cell_{H_2}$ with the increased HER rates (Fig. 3C). The V_{cell} did not change in $Cell_{S_2O_8^{2-}}$ and increased by nearly 350 mV in $Cell_{H_2}$ (Fig. 3C). Although the HER rate increased dramatically, the average CE of RR remained above 99.0 %, the FE of PSR was ~70 %, and the VE of the ModES system was above 91.8 % (Fig. 3D). These results confirm the tolerance and robustness of the decoupled ModES system operated at highly mismatched reaction rates. Consequently, this ModES system could effectively produce H_2 within 2s and

persulfate within 5 min, which makes it feasible to participate in different dynamic electricity markets.

Participation strategies in multiple electricity markets

We developed a computational modeling framework to simulate different electrochemical systems (coupled and decoupled), operating modes (flexible and inflexible power loads), and market participation strategies (Fig. 4A, see more details in figs. S18–26, and supplementary text). This framework allows us to quantify the economic benefits of connecting a flexible, decoupled ModES system to electricity markets operating at different timescales (DAM, RTM, and FR) and at different geographical locations in the PJM (Pennsylvania, Jersey, Maryland) market and in the ERCOT (Electric Reliability Council of Texas) market. All systems and operating modes compared in this study produce the same total amount of chemicals. Fig. 4B shows that the decoupled ModES system that operates under a flexible power load, particularly in PJM and Houston, TX (ERCOT), can reduce electricity costs by as much as 30-40% compared to the baseline system (a coupled system operating under an inflexible/constant power load). In areas with a strong incentive for market flexibility (high frequency of negative prices), such as the RTM in Panhandle, TX (ERCOT), operating under a flexible load can offset or even reverse electricity costs (generating revenue), highlighting the significant economic benefits of providing flexibility to the power grid. The decoupled ModES system has the ability to participate in the fast FR market to generate revenue (due to decoupling of reaction timescales), a flexibility feature that coupled systems cannot provide. To give more perspective on the benefits of participating in FR, we note that allowing the flexible ModES system to simultaneously participate in the DAM and in the FR market can generate up to 0.37 million USD/yr in revenue from the FR market and reduce the total electricity cost by 65% (relative to a flexible ModES system that does not participate in the FR market). A substantial spatial variation in electricity costs was also observed. For instance, in the PJM market, the annual electricity costs reach up to 3.5 million USD/yr, whereas responding to FR signals in Panhandle, TX results in revenue generation. These results not only demonstrate that the flexibility of the decoupled ModES system can unveil new revenue opportunities, but also that such opportunities are strongly affected by electricity market conditions.

We also note that cost reductions require the synchronization of chemical production (anodic and cathodic) with market signals (full details in figs. S23-26). For instance, Fig. 4C shows the chemical production schedule of a coupled system operated with constant power loads. In contrast, in the production schedule for a coupled system operated under flexible loads for the DAM in Houston, TX (Fig. 4D), the anode and cathode production schedules follow the slow dynamics of the DAM market. In the production schedule of the decoupled ModES system (Fig. 4E), it becomes apparent how persulfate production tracks the RTM market dynamics, while hydrogen production tracks the fast FR market dynamics. This separation in production schedules is key for enabling cost reductions.

Conclusions

We developed a modular electrochemical process with highly mismatched reaction rates that can participate in dynamic electricity markets to reduce the cost of electricity consumption for chemical production. Such a strategy is enabled by a fast proton battery material with excellent rate capability and electrochemical stability that delivers high Coulombic efficiency and capacity retention even under highly mismatched charging/discharging rates. The rate-mismatched ModES system achieves the co-production of hydrogen gas and persulfate with reaction rate ratio from 1:1 to 100:1 (when hydrogen production takes less than 2 s) and shows excellent Coulombic and

energy efficiency ~ 100%. Furthermore, the developed computational framework shows that the ModES system operating under a flexible power load reduces electricity cost by 30-40% compared to the traditional coupled system operating under a constant power load. Such a decoupled ModES system can even generate revenue by participating in the FR market, which is impossible in the traditional coupled system. These results provide a new conceptual strategy to help decarbonize the power grid by connecting flexible electrochemical synthesis to dynamic electricity markets and show how the decoupled electrosynthesis can open new revenue opportunities.

References and Notes

1. R. Orvis, S. Aggarwal, A roadmap for finding flexibility in wholesale markets. *San Francisco, CA: Energy Innovation: Policy and Technology LLC*, (2017).
2. B. Kroposki *et al.*, Achieving a 100% renewable grid: Operating electric power systems with extremely high levels of variable renewable energy. *IEEE Power and energy magazine* **15**, 61-73 (2017).
3. Y. Cao, V. M. Zavala, F. D'Amato, Using stochastic programming and statistical extrapolation to mitigate long-term extreme loads in wind turbines. *Applied energy* **230**, 1230-1241 (2018).
4. K. Kim, F. Yang, V. M. Zavala, A. A. Chien, Data centers as dispatchable loads to harness stranded power. *IEEE Transactions on Sustainable Energy* **8**, 208-218 (2016).
5. L. Bird *et al.*, Wind and solar energy curtailment: A review of international experience. *Renew. Sustain. Energy Rev.* **65**, 577-586 (2016).
6. H. Schermeyer, C. Vergara, W. Fichtner, Renewable energy curtailment: A case study on today's and tomorrow's congestion management. *Energy Policy* **112**, 427-436 (2018).
7. A. W. Dowling, R. Kumar, V. M. Zavala, A multi-scale optimization framework for electricity market participation. *Applied Energy* **190**, 147-164 (2017).
8. J. Seel, D. Millstein, A. Mills, M. Bolinger, R. Wiser, Plentiful electricity turns wholesale prices negative. *Advances in Applied Energy* **4**, 100073 (2021).
9. M. Child, C. Kemfert, D. Bogdanov, C. Breyer, Flexible electricity generation, grid exchange and storage for the transition to a 100% renewable energy system in Europe. *Renewable energy* **139**, 80-101 (2019).
10. S. Rehman, L. M. Al-Hadhrami, M. M. Alam, Pumped hydro energy storage system: A technological review. *Renew. Sustain. Energy Rev.* **44**, 586-598 (2015).
11. C.-J. Yang, R. B. Jackson, Opportunities and barriers to pumped-hydro energy storage in the United States. *Renew. Sustain. Energy Rev.* **15**, 839-844 (2011).
12. M. Budt, D. Wolf, R. Span, J. Yan, A review on compressed air energy storage: Basic principles, past milestones and recent developments. *Applied Energy* **170**, 250-268 (2016).
13. H. Lund, G. Salgi, The role of compressed air energy storage (CAES) in future sustainable energy systems. *Energy Conversion and Management* **50**, 1172-1179 (2009).
14. B. Dunn, H. Kamath, J.-M. Tarascon, Electrical Energy Storage for the Grid: A Battery of Choices. *Science* **334**, 928-935 (2011).
15. M. T. Lawder *et al.*, Battery energy storage system (BESS) and battery management system (BMS) for grid-scale applications. *Proceedings of the IEEE* **102**, 1014-1030 (2014).
16. H. S. d. Boer, L. Grond, H. Moll, R. Benders, The application of power-to-gas, pumped hydro storage and compressed air energy storage in an electricity system at different wind power penetration levels. *Energy* **72**, 360-370 (2014).
17. M. Götz *et al.*, Renewable Power-to-Gas: A technological and economic review. *Renewable Energy* **85**, 1371-1390 (2016).

18. J. Ma *et al.*, Exploiting electricity market dynamics using flexible electrolysis units for retrofitting methanol synthesis. *Energ Environ Sci* **16**, 2346-2357 (2023).
19. Y. Cao, S. B. Lee, V. R. Subramanian, V. M. Zavala, Multiscale model predictive control of battery systems for frequency regulation markets using physics-based models. *Journal of Process Control* **90**, 46-55 (2020).
20. A. Sood *et al.*, Electrochemical ion insertion from the atomic to the device scale. *Nat Rev Mater* **6**, 847-867 (2021).
21. L. Chen, X. Dong, Y. Wang, Y. Xia, Separating hydrogen and oxygen evolution in alkaline water electrolysis using nickel hydroxide. *Nat Commun* **7**, 11741 (2016).
22. H. Dotan *et al.*, Decoupled hydrogen and oxygen evolution by a two-step electrochemical–chemical cycle for efficient overall water splitting. *Nat Energy* **4**, 786-795 (2019).
23. A. Landman *et al.*, Photoelectrochemical water splitting in separate oxygen and hydrogen cells. *Nat Mater* **16**, 646-651 (2017).
24. Y. Ma, Z. Guo, X. Dong, Y. Wang, Y. Xia, Organic Proton-Buffer Electrode to Separate Hydrogen and Oxygen Evolution in Acid Water Electrolysis. *Angewandte Chemie Int Ed* **58**, 4622-4626 (2019).
25. B. Rausch, M. D. Symes, G. Chisholm, L. Cronin, Decoupled catalytic hydrogen evolution from a molecular metal oxide redox mediator in water splitting. *Science* **345**, 1326-1330 (2014).
26. M. D. Symes, L. Cronin, Decoupling hydrogen and oxygen evolution during electrolytic water splitting using an electron-coupled-proton buffer. *Nat Chem* **5**, 403-409 (2013).
27. F. Wang *et al.*, Modular Electrochemical Synthesis Using a Redox Reservoir Paired with Independent Half-Reactions. *Joule* **5**, 149-165 (2021).
28. K. H. Michael *et al.*, Pairing of Aqueous and Nonaqueous Electrosynthetic Reactions Enabled by a Redox Reservoir Electrode. *J Am Chem Soc* **144**, 22641-22650 (2022).
29. R. Wang *et al.*, Sustainable Coproduction of Two Disinfectants via Hydroxide-Balanced Modular Electrochemical Synthesis Using a Redox Reservoir. *Acs Central Sci* **7**, 2083-2091 (2021).
30. . (2023), vol. 2023.
31. D. Chao *et al.*, Roadmap for advanced aqueous batteries: From design of materials to applications. *Sci Adv* **6**, eaba4098 (2020).
32. G. Liang, F. Mo, X. Ji, C. Zhi, Non-metallic charge carriers for aqueous batteries. *Nat Rev Mater* **6**, 109-123 (2021).
33. N. Agmon, The Grotthuss mechanism. *Chem Phys Lett* **244**, 456-462 (1995).
34. K. Ono *et al.*, Grain-Boundary-Free Super-Proton Conduction of a Solution-Processed Prussian-Blue Nanoparticle Film. *Angew Chem-ger Edit* **129**, 5623-5627 (2017).
35. S.-i. Ohkoshi *et al.*, High Proton Conductivity in Prussian Blue Analogues and the Interference Effect by Magnetic Ordering. *J Am Chem Soc* **132**, 6620-6621 (2010).
36. H. Jiang *et al.*, Insights on the Proton Insertion Mechanism in the Electrode of Hexagonal Tungsten Oxide Hydrate. *J Am Chem Soc* **140**, 11556-11559 (2018).
37. Z. Zhu *et al.*, An Ultrafast and Ultra-Low-Temperature Hydrogen Gas–Proton Battery. *J Am Chem Soc* **143**, 20302-20308 (2021).
38. X. Wu *et al.*, Diffusion-free Grotthuss topochemistry for high-rate and long-life proton batteries. *Nat Energy* **4**, 123-130 (2019).
39. C. D. Wessells, R. A. Huggins, Y. Cui, Copper hexacyanoferrate battery electrodes with long cycle life and high power. *Nat Commun* **2**, 550 (2011).

40. D. Asakura *et al.*, Bimetallic Cyanide-Bridged Coordination Polymers as Lithium Ion Cathode Materials: Core@Shell Nanoparticles with Enhanced Cyclability. *J Am Chem Soc* **135**, 2793-2799 (2013).
41. J. Wang, J. Polleux, J. Lim, B. Dunn, Pseudocapacitive Contributions to Electrochemical Energy Storage in TiO 2 (Anatase) Nanoparticles. *J Phys Chem C* **111**, 14925-14931 (2007).
42. H.-S. Kim *et al.*, Oxygen vacancies enhance pseudocapacitive charge storage properties of MoO3−x. *Nat Mater* **16**, 454-460 (2016).
43. K. G. Serrano, A critical review on the electrochemical production and use of peroxo-compounds. *Curr. Opin. Electrochem.* **27**, 100679 (2021).
44. S. S. Kumar, V. Himabindu, Hydrogen production by PEM water electrolysis – A review. *Mater. Sci. Energy Technol.* **2**, 442-454 (2019).
45. W. Smit, J. G. Hoogland, The mechanism of the anodic formation of the peroxodisulphate ion on platinum —IV. influence of alkali-metal cations. *Electrochimica Acta* **16**, 981-993 (1971).
46. P. A. Michaud, Preparation of Peroxodisulfuric Acid Using Boron-Doped Diamond Thin Film Electrodes. *Electrochem. Solid-State Lett.* **3**, 77 (1999).

Acknowledgments: The authors acknowledge the facilities and instrumentation at the UW-Madison Wisconsin Centers for Nanoscale Technology (wcnt.wisc.edu), partially supported by the NSF through the University of Wisconsin Materials Research Science and Engineering Center (DMR-1720415).

Funding:

National Science Foundation grant FMRG-2328160 to R. W., J. M., V. Z., and S. J.

National Science Foundation grant CBET-1748516 to J. M. and V. Z.

Wisconsin Alumni Research Foundation to R. W., H. S., and S. J.

Author contributions: R. W., H. S., V. Z., and S. J. conceived the idea and designed the experiments. R. W. carried out materials synthesis, materials characterization, electrochemical measurements, and electrochemical production. J. M. and V. Z. conducted numerical analysis. V. Z. and S. J. supervised the project. R. W., J. M., V. Z., and S. J. wrote the manuscript, and all authors commented on it.

Competing interests: Authors declare that they have no competing interests.

Data and materials availability: The data that support the findings of this study are available from the corresponding authors upon reasonable request. The code and data for the computational framework is available at https://github.com/zavalab/ModES.

Supplementary Materials

Materials and Methods

Supplementary Text

Figs. S1 to S26

Tables S1 to S2

References (38, 47-48)

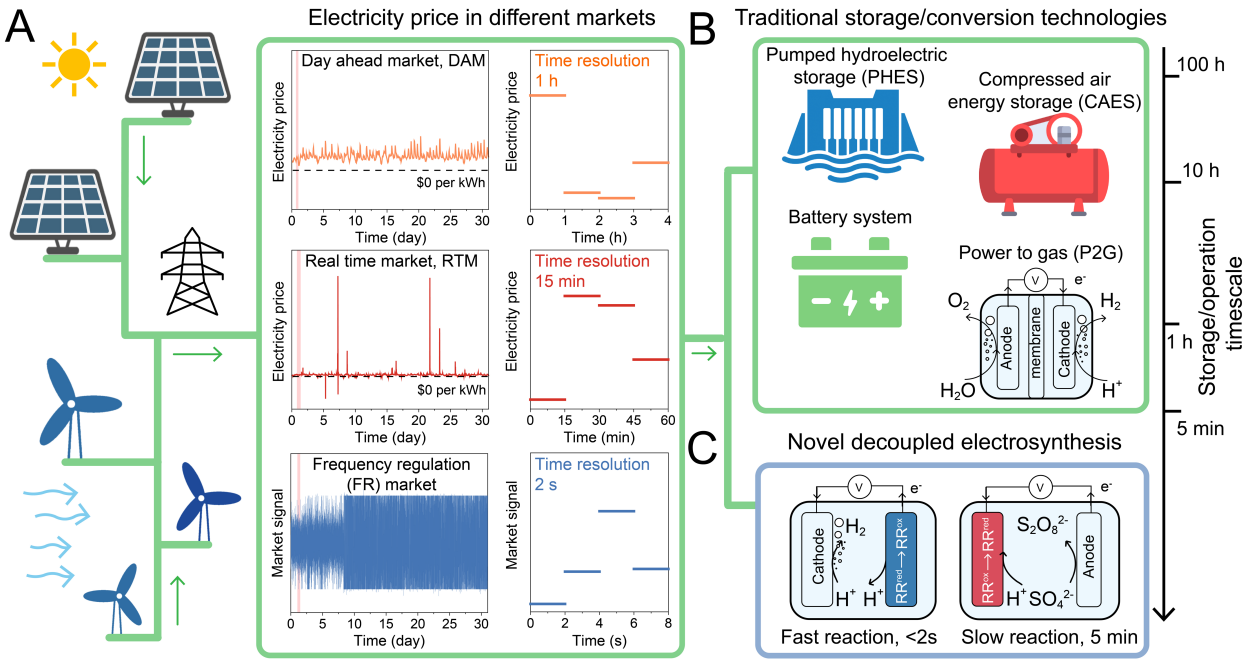

Fig. 1. Participation in dynamic electricity markets using current energy storage or conversion technologies and using our proposed highly rate-mismatched modular electrosynthesis with drastically different storage/operation timescale. (**A**) Different electricity markets are used by independent system operators (ISOs) to balance the power grid and mitigate the risk that results from the variability of solar and wind power at different timescales. For example, the day-ahead market (DAM) with an hour resolution and real-time market (RTM) with a finer time resolution (5 minutes), are used to (re)balance supply/demand by correcting plans. The frequency regulation (FR) market with a time resolution of 2 seconds aims to secure balance at fast timescales. The price signals of these markets indicate when and where resources are most valuable; technologies capable of responding to such signals can benefit economically. (**B**) Flexible technologies with different storage/operation timescale, such as pumped hydroelectric storage (PHES), compressed air energy storage (CAES), battery systems, power to gas (P2G), and decoupled electrosynthesis, could participate in multiple markets and at different times/locations to help the grid absorb wind/solar power and monetize this service. (**C**) The novel decoupled electrosynthesis could effectively participate in the FR market, which is not possible for traditional systems with long storage/duration time.

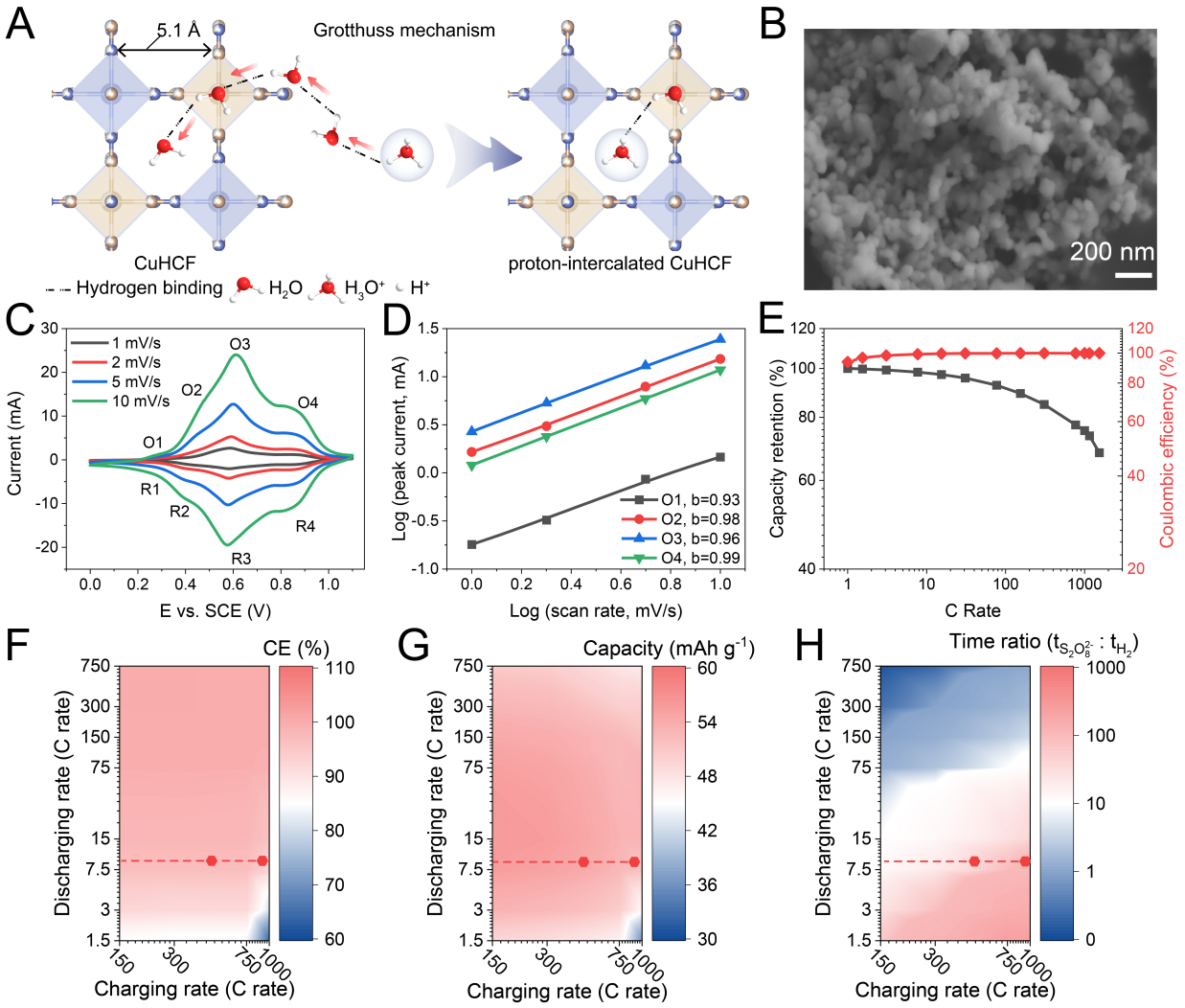

Fig. 2. Structural and electrochemical characterizations of CuHCF as a fast proton battery material. (**A**) Schematic illustration of the Grotthuss mechanism in which protons transport through the hydrogen bond network. (**B**) SEM image of as-synthesized CuHCF nanoparticles. (**C**) Cyclic voltammograms of the CuHCF electrode in 2 M H_2SO_4 solution at 1 mV s^{-1}, 2 mV s^{-1}, 5 mV s^{-1}, and 10 mV s^{-1}. (**D**) Analysis of the anodic peak current (I) as a function of the scan rate (v) in logarithmic scale to extract the exponent b values according to the equation $I = av^b$. (**E**) Rate capability and corresponding Coulombic efficiency of the CuHCF electrode in 2 M H_2SO_4 solution. (**F**) Coulombic efficiencies and (**G**) capacities of the CuHCF electrode at different charging/discharging rates (each panel was interpolated from 32 data points). (**H**) Estimated time ratios of the persulfate production to hydrogen production using the CuHCF electrode at mismatched rates (interpolated from 32 data points). Red dash lines in panels f-h represent targeted mismatched ModES processes with a fixed discharging (PSR) rate of 10C.

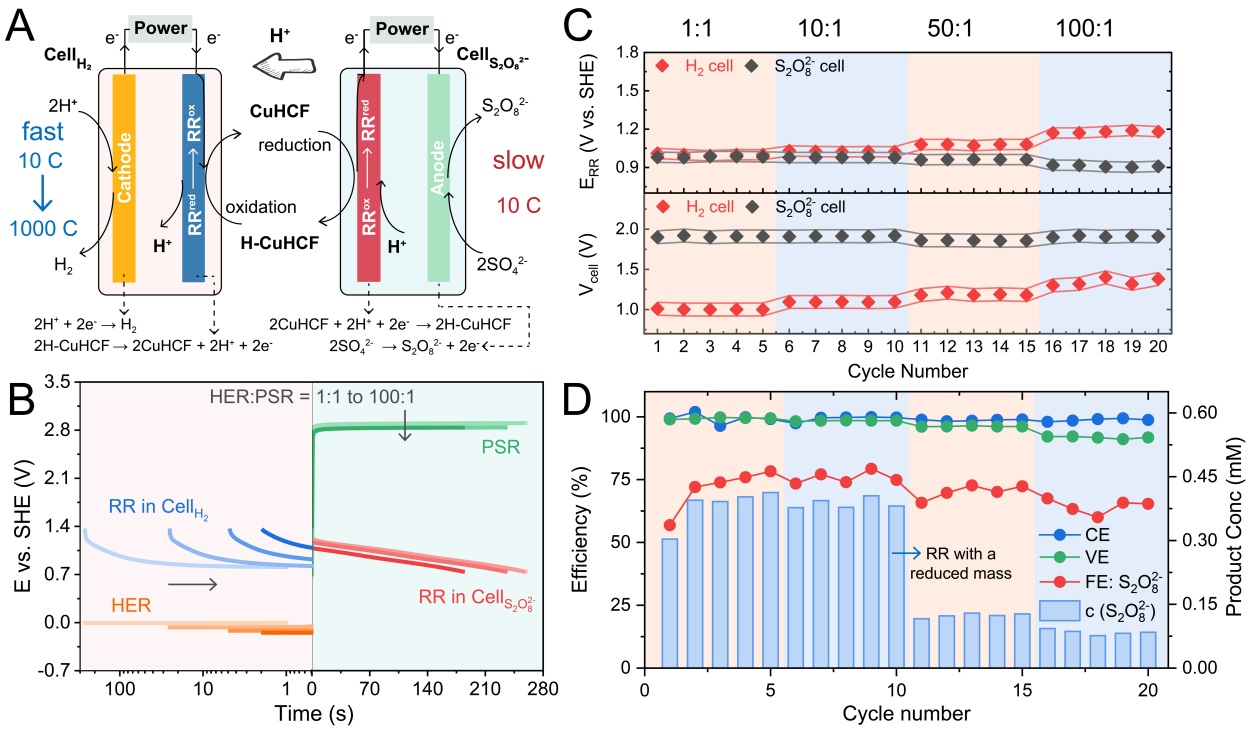

Fig. 3. Modular electrochemical synthesis (ModES) with highly mismatched reaction rates. (**A**) Schematic illustration of the ModES system with highly mismatched reaction rates using CuHCF as the RR, which transports H^+ to pair up sequentially with the HER and PSR reactions in two separate cells, denoted as $Cell_{H_2}$ (left) and $Cell_{S_2O_8^{2-}}$ (right). (**B**) Chronopotentiometry curves of the electrodes in $Cell_{H_2}$ (in logarithmic timescale) and $Cell_{S_2O_8^{2-}}$ (in linear timescale) when the ratio of the HER rate to PSR rate increases from 1:1 to 100:1 following the arrows. Here, the PSR rate at all conditions was 10 C based on the capacity of the RR electrode, and the HER rate increased from 10 C to 100 C, 500 C, and 1000 C. The RR oxidation (blue) was paired with fast HER (orange), and the RR reduction (red) was paired with slow PSR (green), both in 2 M H_2SO_4 solution. (**C**) The average potential of the RR electrode (E_{RR}, top) and the corresponding average cell voltages (V_{cell}, bottom) of $Cell_{H_2}$ and $Cell_{S_2O_8^{2-}}$ in 20-cycle ModES processes under varying ratios of the HER rate to PSR rate from 1:1, 10:1, 50:1, to 100:1. (**D**) Efficiencies (Coulombic efficiency of the RR electrode, voltage efficiency of the ModES process, and Faradaic efficiency of the persulfate production) and the concentrations of accumulated products during the ModES process under different operation conditions (corresponding to the same cycles in panel c).

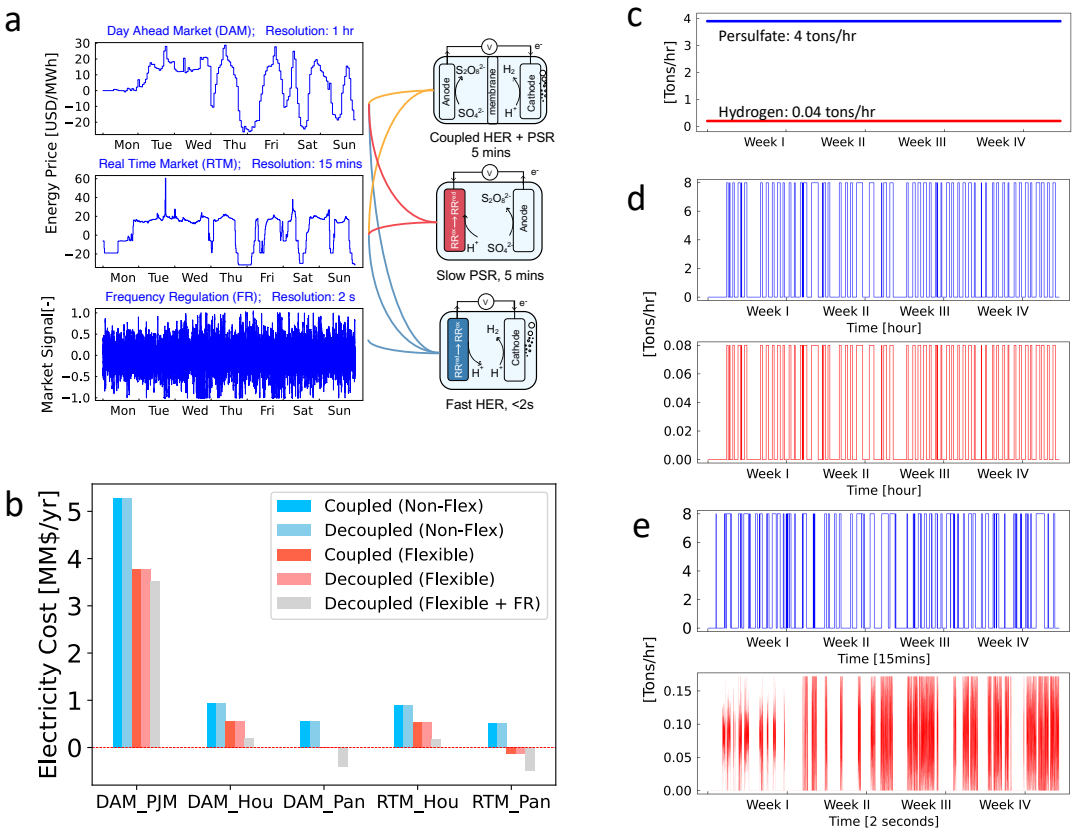

Fig. 4. Market participation strategies and electricity cost reduction. (**A**) Different electricity markets under which coupled and decoupled electrochemical systems can participate. The conventional coupled system can only participate in DAM and RTM because its overall response time is limited by the persulfate production (PSR) and thus this system cannot respond to the fast FR market signals. Decoupled ModES system allows the fast H_2 production (HER) to track FR, DAM, and RTM signals, while the slow PSR can participate in DAM and RTM. (**B**) Quantification of the economic benefits of connecting the ModES system to different markets (DAM, RTM, and FR) and at different locations, including PJM, Houston, TX (ERCOT) and Panhandle, TX (ERCOT). Overall, the use of flexible power loads leads to cost reductions and motivate the need to track market signals. Moreover, decoupling enables cost reductions (in some cases leading to profit) due to participation in the FR market. (**C**) Production schedule of a coupled system operated in constant mode under DAM for PJM. This operating mode is referenced as the *'Coupled (Non-Flex)'* case in Fig. 4B. (**D**) Production schedule for a coupled system showing how DAM market signals are followed to reduce costs. This operation mode corresponds to the *'Coupled (Flexible)'* case in Fig. 4B. (**E**) Production schedule of the decoupled ModES system showing how decoupling enables the anode and cathode to follow markets of different time resolutions to reduce costs. This operation mode corresponds to the *'Decoupled (Flexible+FR)'* case in Fig. 4B.